Journal of Alloys and Compounds 865 (2021) 158948

Contents lists available at ScienceDirect

Journal of Alloys and Compounds

journal homepage: www.elsevier.com/locate/jalcom

Crystallographic, magnetic and magnetocaloric properties in novel intermetallic materials R_3CoNi (R = Tb, Dy, Ho, Er, Tm, Lu)

A. Herrero[a], A. Oleaga[a,*], A. Provino[b,c], I.R. Aseguinolaza[a], A. Salazar[a], D. Peddis[b], P. Manfrinetti[b,c]

[a] Departamento de Física Aplicada I, Escuela de Ingeniería de Bilbao, Universidad del País Vasco UPV/EHU, Plaza Ingeniero Torres Quevedo 1, Bilbao 48013, Spain
[b] Department of Chemistry, University of Genova, Via Dodecaneso 31, Genova 16146, Italy
[c] Institute SPIN-CNR, Corso Perrone 24, Genova 16152, Italy

ARTICLE INFO

Article history:
Received 7 October 2020
Received in revised form 17 December 2020
Accepted 27 January 2021
Available online 30 January 2021

Keywords:
Magnetocaloric effect
Rare earth compound
Magnetic properties
Spin-ordering
Critical behavior

ABSTRACT

A family of novel intermetallic R_3CoNi with heavy rare earth ions has been synthesized (R = Tb, Dy, Ho, Er, Tm, Lu) and a study of the crystal structure of these phases performed. All the compounds adopt the rhombohedral Er_3Ni_2-type structure [Pearson's symbol $hR45$; space group R-3h (N. 148)]. A thorough investigation of their magnetic and magnetocaloric properties has been undertaken. Magnetization and *ac*-susceptibility measurements as a function of temperature show that the samples with Tb, Dy, Ho, Er, and Tm present a paramagnetic to ferromagnetic (PM-FM) transition at temperatures in the range 96–6 K; different reorientation transitions take place below the respective T_C, in most cases with thermomagnetic irreversibility. Thermal and magnetic measurements have been used to retrieve the set of critical exponents (α, β, γ, δ) for the PM-FM transition to assign a universality class to Tb_3CoNi, Dy_3CoNi, and Ho_3CoNi, with the result that, in the first case, it is close to the Mean Field model, in the second one it is between the Chiral Heisenberg and the *XY*-Chiral, and in the third one it is close to the *XY*-Chiral model. Therefore, in Tb_3CoNi the transition is governed by long-range order interactions, whereas in Dy_3CoNi and Ho_3CoNi there must be some kind of frustrated non-collinear ferromagnetism. The magnetocaloric measurements in five members of the family indicate that all of them present highly competitive magnetocaloric properties in their respective temperature ranges, with high magnetic entropy changes (from 12.8 to 18.5 J/Kg.K at $\mu_0\Delta H$ = 5 T) and refrigerant capacities (from 412 to 699 J/Kg at $\mu_0\Delta H$ = 5 T). These results assess and highlight the applicative interest of these compounds, besides suggesting the possibility of tuning the range of the operating temperature by modifying the rare earth ion. Finally, universal curves for the magnetocaloric properties have been found for Tb_3CoNi, Dy_3CoNi, and Ho_3CoNi; the scaling of the magnetocaloric variables confirms the validity of the assigned universality classes.

© 2021 The Author(s). Published by Elsevier B.V.
CC_BY_4.0

1. Introduction

Novel intermetallic materials are being synthetized by many research groups in the world in search of relevant magnetic properties for technological applications. One of the main application fields is magnetic refrigeration making use of the magnetocaloric effect, with the aim to complement or substitute the classical gas compressor-expansion cycles [1–3]. To this end, the magnetic transitions in these materials must present certain particular properties such as a relevant magnetic entropy change (or adiabatic temperature change), broad temperature working range, high refrigerant capacity and, in case of first order transitions, negligible thermal and magnetic hysteresis. Another relevant issue is the temperature of the maximum of the magnetic entropy change as it will affect the practical application. In spite of the fact that, nowadays, room temperature devices are the ones most looked for, there is also a need for materials operating in other temperature regions, such as the gas liquefaction ranges [4–8]. The focus of this work is placed on the latter region, for which we have synthetized and studied the intermetallic family R_3CoNi where R is a heavy rare earth atom R = Tb, Dy, Ho, Er, Tm, and Lu. So far, only the structure and some magnetic properties of Gd_3CoNi [9] and Tb_3CoNi [10] have been investigated, the rest of the series being a complete novelty. As it happens in many other families of rare earth intermetallics, such as *RTX* (R = rare earth, T = transition metal, X = p-block element) [11,12],

* Corresponding author.
E-mail address: alberto.oleaga@ehu.es (A. Oleaga).

https://doi.org/10.1016/j.jallcom.2021.158948
0925-8388/© 2021 The Author(s). Published by Elsevier B.V.
CC_BY_4.0

R_6TX_2 [13–15], R_3Co [16], in Tb_3CoNi the transition metals do not contribute to the net magnetic moment [10]; therefore, the magnetism only arises due to the spin ordering of the *R* atoms. The aim of this work is to study in detail the magnetic properties of this ordering in the first five members of the aforementioned series, paying special attention to the magnetocaloric properties (maximum entropy change, refrigerant capacity, and universal curves) and get a deeper insight into the magnetism of the paramagnetic to ferromagnetic phase transitions by means of the study of their critical behavior, when possible. We will look for the set of critical exponents (α, β, γ, δ, n) which describes the critical behavior of the standard physical variables specific heat, spontaneous magnetization, inverse of the initial susceptibility, critical isotherm, and maximum of the magnetic entropy change, respectively. The correspondence of those sets with a particular universality class will provide information about the spin ordering and dimensionality of the transition [17–21].

2. Samples synthesis and characterization, experimental techniques

Samples with nominal composition R_3CoNi were synthesized for the heavy rare-earths Tb, Dy, Ho, Er, Tm, and Lu. The alloys, in the form of a polycrystalline material, were prepared by arc melting, with the elements taken in stoichiometric proportions under a TiZr-gettered Ar atmosphere (total weight of 3–4 g). The starting constituents were commercial high purity metals: 99.9 wt% purity for the *R* metals (Koch-Light Laboratories Ltd. England), 99.99 wt% purity for both Co and Ni (REacton Alfa, Johnson Matthey GmbH. Germany). After first melting for reaction, the buttons were remelted other three times, turning them upside down each time, to ensure homogeneity. Weight losses after the melting procedure were less than 0.4% (except for Tm; in this case losses were within 1.0%). The small ingots were wrapped in an outgassed Ta foil, sealed under vacuum in quartz tubes and annealed in a resistance furnace. Due to the formation of these phases, likely occurring by a peritectic reaction, the thermal annealing was generally performed in two steps: 680 °C + 700 °C for Tb_3CoNi (for which a formation through a peritectic reaction occurring at 720 °C is reported) [10], and 700 °C + 730 °C for the other R_3CoNi samples (3–4 days each step, for a total of 7–8 days).

The homogeneity of the alloys was checked, and phase analysis performed by optical microscopy (LOM) on micrographic specimens prepared with standard methods and powder X-ray diffraction (XRD). The XRD patterns were recorded on a Guinier camera (Cu Kα1 radiation), using pure Si as an internal standard [a = 5.4308(1) Å]; they were indexed by comparison with the ones calculated by the Lazy PULVERIX program [22]; then, the lattice parameters were determined by means of a least-squares method. The refinement of the crystal structure was performed for Ho_3CoNi, Er_3CoNi and Tm_3CoNi by the Rietveld refinement program FULLPROF [23]. In this case powder XRD data were recorded on a Philips diffractometer (Cu Kα radiation), in the 2θ range of 10°–100°, with steps of 0.02° and counting time of 26–28 s/step.

Magnetic measurements have been performed using a Vibrating Sample Magnetometer by Cryogenic Limited, obtaining first the ZFC, FC, FW magnetization curves from 2 K to room temperature. Once the magnetic transitions have been located, the magnetization (M) of the samples under external applied magnetic fields H_a in the range of 0–7 T has been measured. For all samples, isotherms have been collected from 2 K to temperatures well above the corresponding Curie temperature (T_C), using different steps, depending on the temperature range. In order to study in detail the critical behavior of the paramagnetic to ferromagnetic transition, a step of ΔT = 1 K has been taken between consecutive isotherms around T_C; moreover, to perform a correct evaluation of the magnetocaloric effect and the scaling analysis, demagnetization effects have been taken into account [24,25]. For this purpose, the demagnetization factor *N* has been obtained by means of *ac* susceptibility measurements [26,27], and the internal magnetic field has afterwards been calculated using the equation $H_i = H_a - NM$. The magnetic susceptibility has been measured with the AC Measurement System Option in a Physical Properties Measurement System (PPMS) by Quantum Design. The values of *N* for the three samples are 41.57 gOe/emu for Tb_3CoNi, 43.95 gOe/emu for Dy_3CoNi and 48.99 gOe/emu for Ho_3CoNi.

The specific heat c_p has been retrieved using a high resolution *ac* photopyroelectric calorimeter in the back detection configuration, which allows to perform extremely slow temperature ramps in order to extract the detailed shape of c_p [28–30]. Unfortunately, the lowest temperature that this system can achieve is 15 K, so it has not been possible to obtain these data for all samples, as it will be shown later on.

3. Experimental results and discussion

The series of ternary phases R_3CoNi have been prepared. The room temperature X-ray data reveal that besides Gd [9] and Tb [10] all the heavy *R* down to Lu also form a ternary R_3CoNi compound. The synthesis of an homologous 'Yb_3CoNi' was not attempted in the course of the present study. While Gd_3CoNi [9] adopts the monoclinic Dy_3Ni_2-type (*mS*20; space group *C*2/*m*, N. 12) [31], all compounds formed by the other heavy *R* (Tb to Tm, and Lu) crystallize with the rhombohedral Er_3Ni_2-type structure (Pearson symbol *hR*45; space group *R*-3*h*, N. 148) [32]. This means that not only for Tb_3Ni_2 but in Dy_3Ni_2 and Ho_3Ni_2 as well, the structure changes from the Dy_3Ni_2-type to the Er_3Ni_2-type when partially replacing Ni by Co (to the equiatomic ratio). The lattice parameters (*a* and *c*), unit cell volume (V_{obs}) and volume contraction in the formation of compounds ΔV % {where $\Delta V = [((V_{obs}-V_{calc})/V_{calc})^*100]$; V_{calc} is the volume of the compound calculated from the atomic volumes of the individual atoms [33]} are collected in Table 1. Both the lattice parameters and unit cell volume linearly decrease from Tb down to Lu, well following the lanthanide contraction trend (see Fig. 1).

Rietveld plots concerning the refinement of the crystal structure for Ho_3CoNi, Er_3CoNi and Tm_3CoNi are shown in Fig. 2; the resulting structural data and atomic positions, along with agreement factors, are collected in Tables S1 to S3 (see supplementary material), for the Ho, Er and Tm compounds, respectively.

Fig. 3a shows the magnetization as a function of temperature, both in Zero-Field Cooled (ZFC) and Field-Cooled (FC) mode for the five magnetic samples (*R* = Tb, Dy, Ho, Er, and Tm), with an applied field of 100 Oe. In all cases (except for Tm_3CoNi) there is a clear divergence between the ZFC and FC curves, showing thermomagnetic irreversibility, typical of many ferro/ferrimagnetic transitions. Fig. 3b shows the real part of the *ac* susceptibility, which is a very helpful tool to precisely locate the critical temperatures. With the combination of both magnitudes we see that there is a

Table 1
Lattice parameters (*a* and *c*), observed unit cell volume (V_{obs}) and volume contraction in formation of the phase (ΔV %) for the R_3CoNi compounds (*R* = Tb–Tm, Lu); all crystallizing in the rhombohedral Er_3Ni_2-type (Pearson's symbol *hR*45, space group *R*–3 *h*; Z = 9). Data are from Guinier patterns.

R_3CoNi	Lattice parameters		V_{obs} [Å^3]	ΔV %
	a [Å]	*c* [Å]		
Tb_3CoNi	8.6062(3)	15.679(1)	1005.72	−5.62
Dy_3CoNi	8.5638(7)	15.618(2)	991.96	−5.45
Ho_3CoNi	8.5268(5)	15.563(2)	979.95	−5.62
Er_3CoNi	8.4840(5)	15.561(2)	969.99	−5.40
Tm_3CoNi	8.4500(3)	15.453(1)	955.55	−5.47
Lu_3CoNi	8.3856(4)	15.397(2)	937.63	−5.73

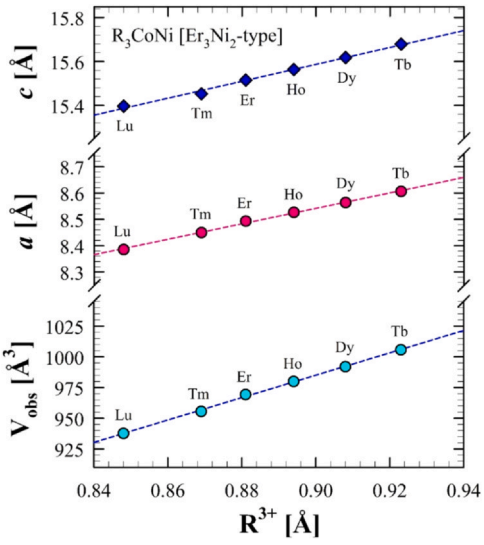

Fig. 1. Trend of the lattice parameters (a and c) and observed unit cell volume (V_{obs}) as a function of the R^{3+} ionic radius for the R_3CoNi compounds (rhombohedral Er_3Ni_2-type; $hR45$, $R{-}3\,h$).

paramagnetic to ferromagnetic (PM-FM) transition at 96 K in the case of Tb_3CoNi, with a nearly identical shape of the magnetization to the one published in [10]. The small peak at about 75 K in the FC curve is surely due to a spin reorientation transition. In fact, in [10] it was observed by neutron diffraction data that, while below T_C the arrangement of the three Tb sublattices is ferromagnetic with components of the magnetic moments in the directions of the a and c vectors (though not completely collinear), at 3.5 K the magnetic moments were on the ab-plane for the now 5 different Tb sublattices, with a canted contribution along the c-direction for 3 of them.

Dy_3CoNi and Ho_3CoNi present similar features with T_C at 53 K and 26 K, respectively. At lower temperatures in each case, there is also a hint of a spin reorientation transition, signalled by the small maximum in the former and a change in slope in the latter in the FC curves (Fig. 3a). Er_3CoNi also presents thermomagnetic irreversibility but there are two clear maxima in the ac susceptibility, at 15 K and 7 K, indicating two different transitions, the first one being the PM-FM while the second one is probably a spin reorientation transition. Finally, Tm_3CoNi has a very small magnetic irreversibility and T_C is located at 6 K but there is the trace of another maximum at a temperature lower than 2 K in the susceptibility.

The thermomagnetic irreversibility and its evolution with the change in rare earth is confirmed by the hysteresis cycles at 2 K, which are shown in Fig. 4, where the coercive field is reduced as the atomic number is increased. In the particular case of Tb_3CoNi the cycle clearly shows the presence of metamagnetic transitions (not seen in the cycles for the other four samples), indicating the presence of strong antiferromagnetic components at very low temperature. Nevertheless, as it will be shown when discussing the magnetocaloric properties, a small antiferromagnetic behavior at low temperature and field is also present in Dy_3CoNi and Er_3CoNi, with a very slight presence in Ho_3CoNi.

Thermomagnetic irreversibility is a phenomenon found in spin glasses, ferromagnetic materials with magnetocrystalline anisotropies, and materials with competing magnetic interactions [34–36]. The features shown in the hysteresis cycles at 2 K in Fig. 4 (coercive fields, metamagnetic transitions in Tb_3CoNi) support the possibility of magnetocrystalline anisotropies at low temperature, which would induce a strong narrow-domain-wall pinning [35], as it happens in many other materials [35,37–39].

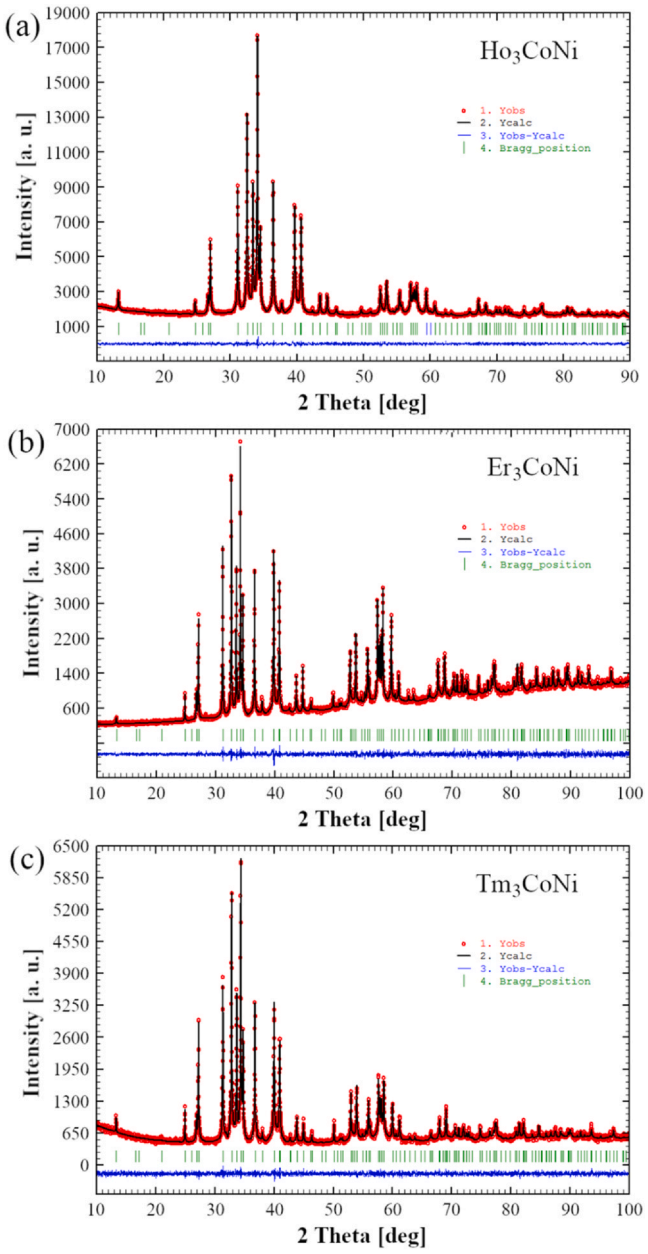

Fig. 2. Observed X-ray powder pattern (red circle) and Rietveld refinement profile (black line) for the samples with nominal composition $Ho_{60}Co_{20}Ni_{20}$ (Fig. 2a); $Er_{60}Co_{20}Ni_{20}$ (Fig. 2b); $Tm_{60}Co_{20}Ni_{20}$ (Fig. 2c). The Bragg angle positions are indicated by vertical bars (green); the lower profile (blue line) gives the difference between observed and calculated data.

3.1. Critical behavior

As mentioned in the introduction, several physical variables present a critical behavior in the near vicinity of the critical temperature of second order phase transitions, fulfilling the following equations as a function of the reduced temperature $t=(T-T_C)/T_C$ [17]: for the spontaneous magnetization $M_S(T)$

$$M_S(T)\sim|t|^{\beta} \qquad (T<T_C), \tag{1}$$

the inverse of the initial susceptibility

$$\chi_0^{-1}(T)\sim|t|^{\gamma} \qquad (T>T_C), \tag{2}$$

and the magnetization at the critical temperature

$$M(H)\sim H^{1/\delta}(T=T_C), \tag{3}$$

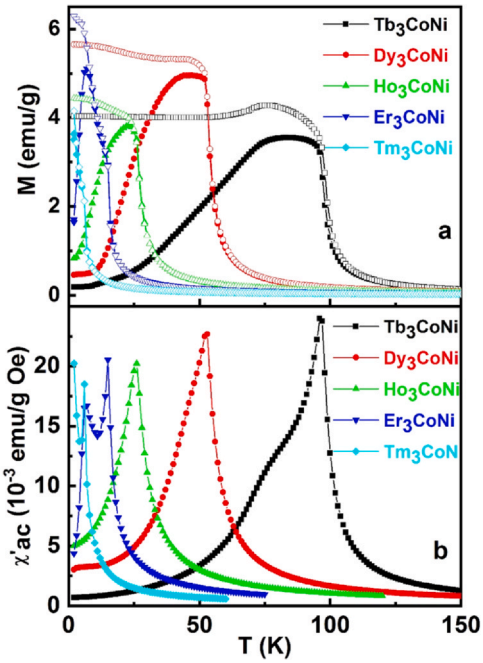

Fig. 3. a) Magnetization as a function of temperature in zero-field cooled (filled-in symbols) and field-cooled (empty symbols) mode with applied field $\mu_0 H = 100$ Oe; b) Real part of the *ac* susceptibility at $f = 100$ Hz.

while the magnetic equation of state

$$M(H, t) = |t|^{\beta} f_{\pm}(H/|t|^{\beta+\gamma}) \tag{4}$$

must be fulfilled in the critical region.
Finally, for the specific heat

$$c_p(T) \sim A^{\pm} |t|^{-\alpha} (A^{-} for T < T_C, A^{+} for T > T_C), \tag{5}$$

This section is devoted to the obtention of these critical exponents (α, β, γ, δ) for the PM-FM transitions in Tb_3CoNi, Dy_3CoNi, and Ho_3CoNi. In the case of Er_3CoNi, the presence of a second transition very close to it (7 K versus 15 K) makes it impossible to isolate the critical behavior of the PM-FM one. A similar situation is found for Tm_3CoNi.

For the magnetic exponents, a customary procedure has been followed [40,41]. From now on, and in order to maintain a notation as simple as possible, H will be used instead of H_i to represent the internal field. As a starting point for the analysis, the standard Arrott Plot (M^2 isotherms as a function of H/M in the near vicinity of T_C) has been drawn, as well as the Modified Arrott Plots (MAP), plotting $M^{1/\beta}$ versus $(H/M)^{1/\gamma}$ for the Heisenberg ($\beta = 0.3689(3)$, $\gamma = 1.3960(9)$) [42] and Ising universality classes ($\beta = 0.32653(10)$, $\gamma = 1.2373(2)$) [43]. The standard Arrott Plot corresponds to the case of the Mean Field universality class ($\beta = 0.5$, $\gamma = 1$). The case which presents, as a whole, a better bunch of straight and parallel lines is taken as the starting point for the analysis. In the case of Dy_3CoNi and Ho_3CoNi the Ising model has been the starting point while in Tb_3CoNi additional pairs for β and γ have been checked (since the linearity in the general (Modified) Arrott plots was not good enough with the three previous models), with the result that the best one as starting point has been $\beta = 0.38$, $\gamma = 1.1$ (see Figs. S1, S2, S3 in the supplementary material, which contain the comparison of the relative slopes for the different trial models). Starting from the one in which the curves at high fields are straighter and more parallel among them, the usual iterative process to find the best values for β and γ has been followed: a linear extrapolation of these isotherms has been taken from the high field values to extract $(M_S)^{1/\beta}$ and $(\chi_0^{-1})^{1/\gamma}$ as an intercept on $M^{1/\beta}$ and $(H/M)^{1/\gamma}$ axis, respectively. These values of $M_S(T)$ and $\chi_0^{-1}(T)$ have been independently fitted to

$$M_S(T) \sim |t|^{\beta} (T < T_C), \tag{6}$$

$$\chi_0^{-1}(T) \sim |t|^{\gamma} (T > T_C), \tag{7}$$

respectively, thus extracting new values of β and γ. With these values new MAPs are drawn, new extrapolations are done, new fittings to Eqs. (6) and (7) are performed and so forth till the values of the critical exponents converge and the best parallelism is obtained in the MAPs. Fig. 5 shows the result of this iterative process for the three samples (3 rounds were enough for Ho_3CoNi, 2 rounds for Tb_3CoNi and Dy_3CoNi) and Table 2 contains the critical exponents thus obtained with their uncertainties.

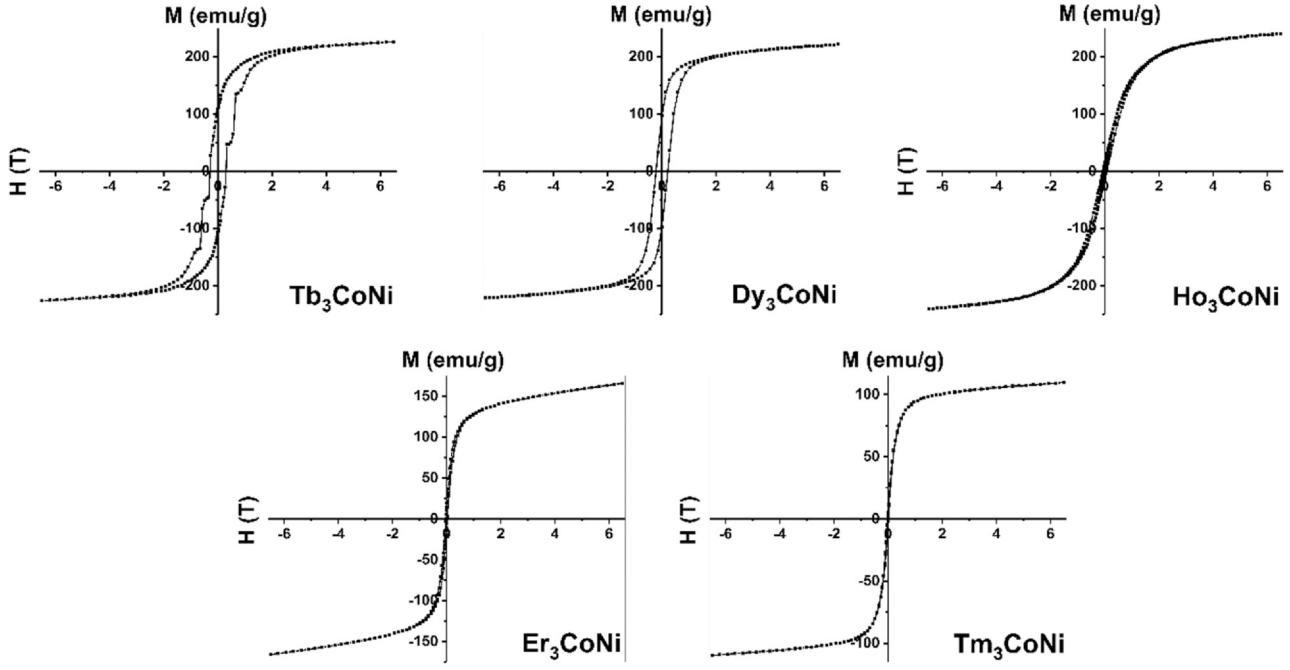

Fig. 4. Hysteresis loops at 2 K for the five R_3CoNi magnetic samples.

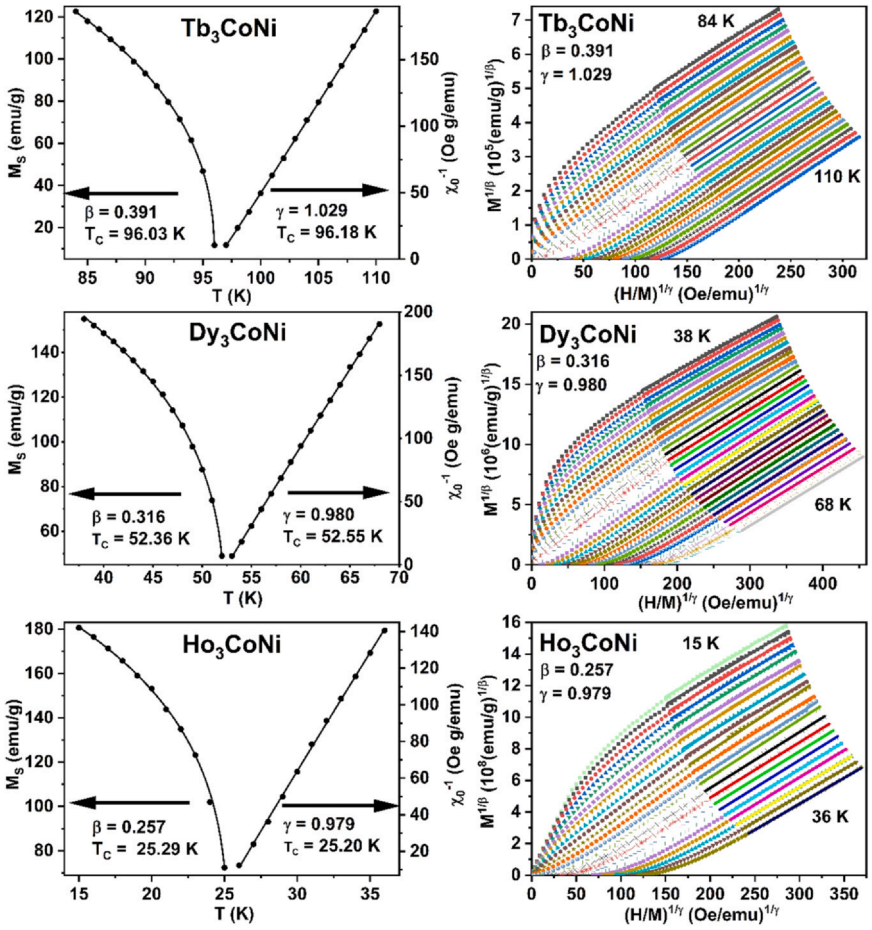

Fig. 5. Left column: Spontaneous magnetization (left) and inverse of initial susceptibility (right) vs. temperature for Tb_3CoNi, Dy_3CoNi, and Ho_3CoNi. The solid curves correspond to the fits to Eqs. (6) and (7), as explained in the text. Right column: optimized Modified Arrot Plots.

Table 2
Critical exponents obtained for Tb_3CoNi, Dy_3CoNi, and Ho_3CoNi.

Material	Technique	β	γ	δ	α	A^+/A^-
Tb_3CoNi	Modified Arrott Plot	0.391 ± 0.002 T_C = 96.03 ± 0.01 K	1.03 ± 0.01 T_C = 96.18 ± 0.06 K	3.63[a] ± 0.04		
	Kouvel-Fisher Method	0.387 ± 0.007 T_C = 95.94 ± 0.02 K	1.02 ± 0.02 T_C = 96.23 ± 0.09 K	3.6[a] ± 0.1		
	Critical Isotherm			3.64 ± 0.01		
	Specific Heat				≈0	–
Dy_3CoNi	Modified Arrott Plot	0.316 ± 0.003 T_C = 52.36 ± 0.03 K	0.98 ± 0.08 T_C = 52.55 ± 0.05 K	4.11[a] ± 0.05		
	Kouvel-Fisher Method	0.300 ± 0.006 T_C = 52.07 ± 0.04 K	0.95 ± 0.02 T_C = 52.72 ± 0.09 K	4.2[a] ± 0.1		
	Critical Isotherm			4.17 ± 0.01		
	Specific Heat				+0.33 ± 0.04	0.62
Ho_3CoNi	Modified Arrott Plot	0.257 ± 0.003 T_C = 25.29 ± 0.02 K	0.98 ± 0.03 T_C = 25.2 ± 0.1 K	4.8[a] ± 0.2		
	Kouvel-Fisher Method	0.245 ± 0.009 T_C = 25.13 ± 0.04 K	0.94 ± 0.03 T_C = 25.3 ± 0.1 K	4.8[a] ± 0.3		
	Critical Isotherm			4.75 ± 0.02		
	Specific Heat				+0.30 ± 0.01	2.5

[a] Calculated from Eq. (8) $\delta = 1 + \gamma/\beta$.

As a second step, the Kouvel-Fisher analysis has been undertaken, which assesses that $M_S(dM_S/dT)^{-1}$ and $\chi_0^{-1}(d\chi_0^{-1}/dT)^{-1}$ have a linear behavior with respect to T, with slopes $1/\beta$ and $1/\gamma$, respectively. Fig. 6 shows these data and the corresponding fittings, from which new β and γ are obtained, giving values very close to the previous ones for each material. In this analysis, the Curie temperature is found from the intercept of the straight fitted lines on the temperature axis. Table 2 gathers again all these results.

Then, for the three compounds, the critical isotherms have been plotted to extract the critical exponent δ, after Eq. (3). Fig. 7 shows them in a log-log scale. In this form, a fit to a linear function easily gives the value of δ, which can be compared with the one calculated using the experimentally found β and γ and the Widom scaling equation [17]:

$$\delta = 1 + \gamma/\beta \tag{8}$$

It can be appreciated in Table 2 that, in each case, the agreement between the experimental and calculated δ is very good.

It is generally accepted that the fulfilment of the magnetic equation of state Eq. (4) is a severe confirmation of the validity of these critical exponents to describe the magnetic transition. This equation of state is shown in Fig. 8 for the three cases where, for each of them, all isotherms collapse onto two independent branches,

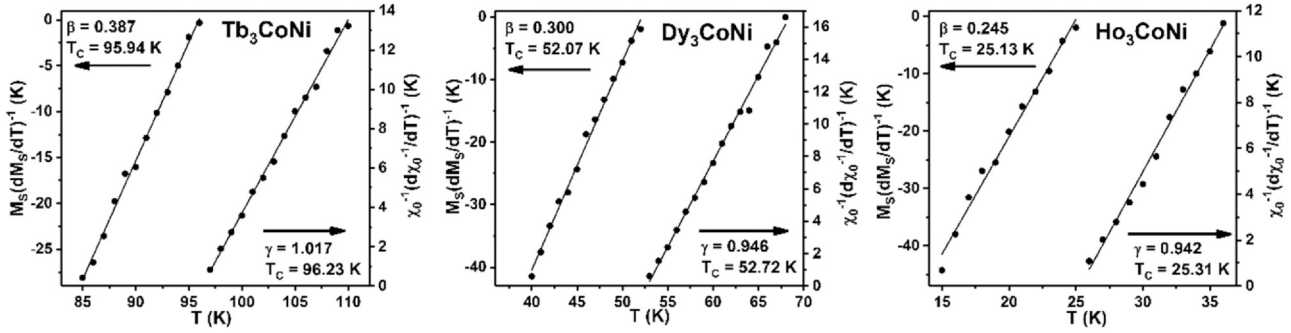

Fig. 6. Kouvel-Fisher plot of spontaneous magnetization (left) and inverse of initial susceptibility (right) for each compound: Tb_3CoNi, Dy_3CoNi, and Ho_3CoNi. The straight lines are linear fits, from which T_C and the critical exponents are obtained.

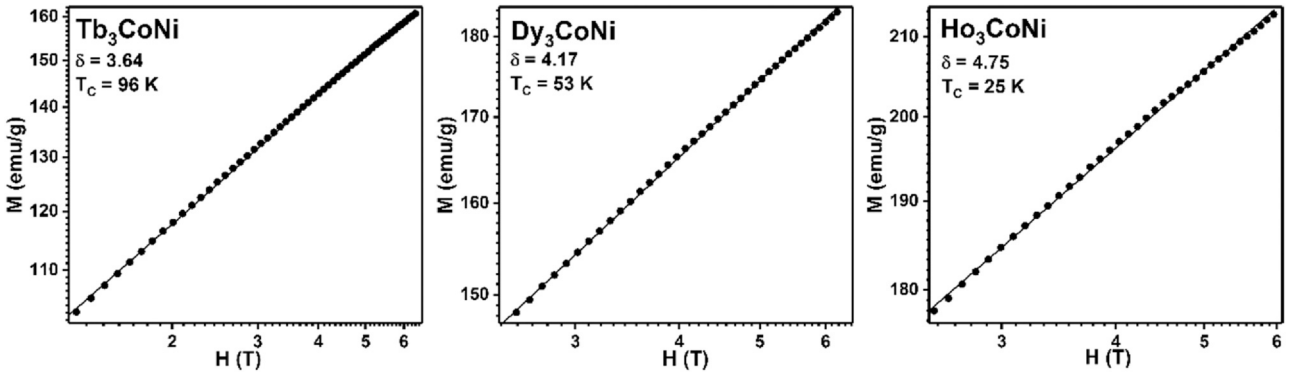

Fig. 7. M vs. H plot in a log-log scale collected at critical isotherms for Tb_3CoNi, Dy_3CoNi, and Ho_3CoNi (from left to right). The straight line, in each case, is the linear fit from which the exponent δ is obtained.

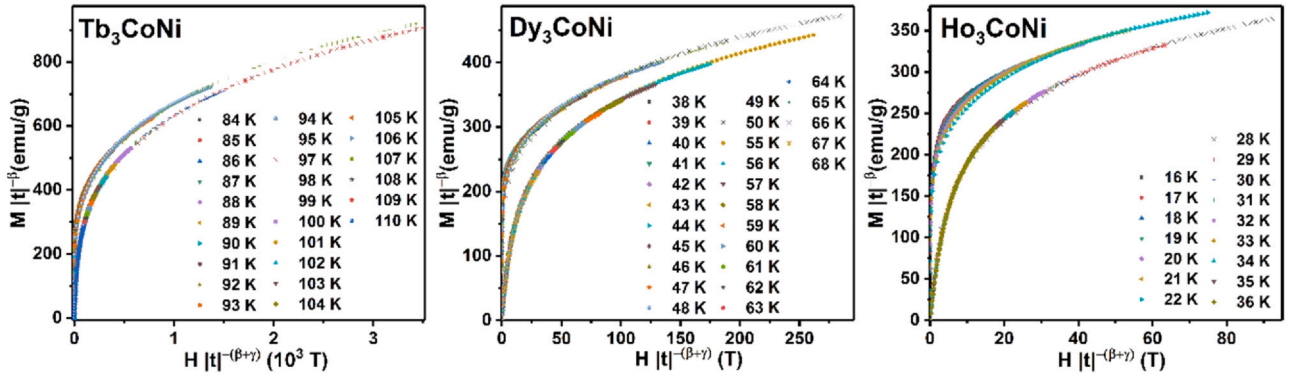

Fig. 8. The renormalized magnetization plotted as a function of the renormalized field following Eq. (4) for Tb_3CoNi, Dy_3CoNi, and Ho_3CoNi (from left to right). In the three cases, the data collapse onto two separate branches, one above and one below the respective T_C.

one for those above T_C, another for those below it, as it is theorized for the right critical exponents.

Let's now turn our attention to the critical behavior of specific heat. The function customarily used to fit the experimental curves of this magnitude is [44,45]:

$$c_p = B + Ct + A^{\pm}|t|^{-\alpha}(1 + E^{\pm}|t|^{0.5}) \tag{9}$$

where t is the reduced temperature and α (the critical exponent), $A^{\pm}$, B, C and $E^{\pm}$ are adjustable parameters. Superscripts + and − stand for $T > T_C$ and $T < T_C$ respectively.

In the particular case in which the Mean Field model is of application ($\alpha = 0$), the critical equation would take an asymptotical logarithmic form at the paramagnetic phase, while the ferromagnetic phase may be described by a Landau classical formulation. As a consequence, the paramagnetic region is fitted to

$$c_p = A \ln t + B + Ct \tag{10}$$

whereas the ferromagnetic one is fitted to

$$c_p = A_1 \frac{T}{\sqrt{1 - 4A_2(T - T_C)}} + B' + C'(T - T_C) \tag{11}$$

[46]. The particulars on how this standard fitting procedure is carried out are described elsewhere [29,45,46].

Fig. 9 shows the experimental specific heats, the fittings and the deviation plots (the latter contain the difference between the experimental and the fitted points, in percentage). The best fittings for Dy_3CoNi and Ho_3CoNi have been obtained by using Eq. (9), with the resulting values of $\alpha = +0.33 \pm 0.04$ and $\alpha = +0.30 \pm 0.01$, respectively. Another parameter which is also predicted by the universality classes is the ratio A^+/A^-, whose values from the fittings are 0.62 for Dy_3CoNi and 2.5 for Ho_3CoNi (though, as the rounding is quite severe, it is not too

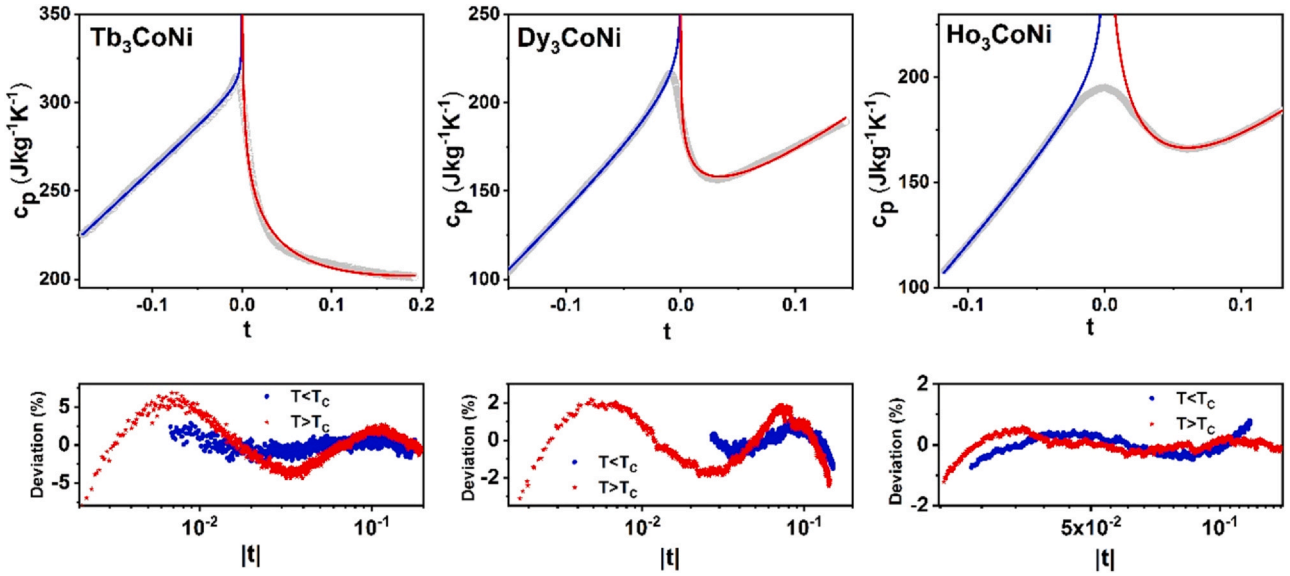

Fig. 9. Top line: Experimental (grey open circles) and fitted curves (continuous lines) of the specific heat as a function of the reduced temperature for the three compounds in the near vicinity of T_C. Bottom line: deviation plots for the fittings (difference between the experimental points and the fittings, in percentage) where blue circles correspond to $T < T_C$, red stars for $T > T_C$.

reliable). For Tb_3CoNi, the best fitting has been obtained with the use of Eqs. (10) and (11), implying that the critical exponent α tends to zero.

All the critical parameters found for Tb_3CoNi, Dy_3CoNi, and Ho_3CoNi have been collected in Table 2, while Table 3 presents the sets of critical exponents for a number of universality classes which might be worth considering [17,42,43,47–56], taking into account the contents of Table 2.

In the particular case of Tb_3CoNi, the value of γ and the fitting of the specific heat agree quite well with the mean field model while β and δ are in between the 3D-Heisenberg and the Mean Field model. This would suggest that the PM-FM transition in this case would belong to the Mean Field model, indicating that long range order interactions are responsible for this transition but with a certain deviation from it. Renormalization group analysis maintains that the range of the exchange interaction $J(r)$ is determined by the critical parameter γ by means of the dependence [57].

$$J(r) \sim r^{-(d+\sigma)} \tag{12}$$

where d is the dimension of the system, r the distance and σ the range of the exchange interaction, where the relation between the latter and γ is:

$$\gamma = 1 + \frac{4}{d}\left(\frac{n+2}{n+8}\right)\Delta\sigma + \frac{8(n+2)(n-4)}{d^2(n+8)^2}\left[1 + \frac{2G\left(\frac{d}{2}\right)(7n+20)}{(n-4)(n+8)}\right]\Delta\sigma^2 \tag{13}$$

Table 3
Set of critical exponents and ratios for several universality classes. d dimensionality of the interaction, n number of spin components, α and A^+/A^- are those of specific heat, β of spontaneous magnetization, γ of isothermal susceptibility, δ of critical isotherm [17,42,43,47–56].

Universality class	d	n	α	β	γ	δ	A^+/A^-
Mean-field Model	–	–	0	0.5	1.0	3.0	–
3D-Ising	3	1	0.11	0.3265	1.2373	4.79	0.53
3D-XY	3	2	−0.014	0.34	1.30	4.82	1.06
3D-Heisenberg	3	3	−0.134	0.3689	1.3960	4.80	1.52
XY-Chiral	3	2	0.34	0.253	1.13		0.36
Chiral-Heisenberg	3	3	0.24	0.30	1.17		0.54
Tricritical Mean Field	–	–	0.5	0.25	1.0	5	–

where $\Delta\sigma = \sigma - d/2$, $G\left(\frac{d}{2}\right) = 3 - \frac{1}{4}\left(\frac{d}{2}\right)^2$, being n the spin dimensionality. In this case, with $\gamma = 1.03$, the resulting value is $\sigma = 1.56$. Long range interaction corresponds to $\sigma = 1.5$, while, for instance, for the short-range 3D-Heisenberg universality class, $\sigma = 2$ [57]. This result further confirms that the magnetic interactions are closer to a long range interaction rather than to short range ones.

In the case of Dy_3CoNi, β and γ agree quite well with the Chiral Heisenberg; the sign of α and the ratio A^+/A^- also agree with it, though the value of α agrees better with the *XY*-Chiral; as a whole, the complete set of exponents is between the two Chiral models. Finally, in the case of Ho_3CoNi, there are three exponents (α, β and γ) whose values are quite close to the *XY*-Chiral model.

These critical exponents imply that Dy_3CoNi and Ho_3CoNi are not common collinear ferromagnets but a certain kind of frustrated non-collinear magnets. Renormalization group theories and Monte-Carlo approaches have been used to study the symmetry and the corresponding critical exponents of frustrated non-collinear magnets, among which are the stacked triangular antiferromagnets (such as the vanadium dihalides VCl_2, VBr_2 or $CsMnBr_3$, $CsVCl_3$) or the helical magnets (such as pure Dy and Ho), developing what is known as the *XY*-Chiral class, whose critical exponents can be found in Table 3 [51,53–56]. Experimental measurements on all these materials have shown that they belong to the *XY*-Chiral universality class [58–60].

The low ordering temperature from the paramagnetic phase indicates the degree of magnetic frustration which takes place in R_3CoNi. The magnetic properties in this system mainly arise from the rare earth (it has been established in Tb_3CoNi that neither Co nor Ni present magnetic moment [10]) though the ordering temperatures are much lower than in the case of the pure systems where the spins take an helical arrangement (179 K in Dy, 132 K in Ho [61]). Without neutron diffraction measurements, it is not possible to ascertain which the spins arrangement is in Dy_3CoNi or Ho_3CoNi; however, the critical exponents here obtained suggest some kind of non-collinearity as it happens in pure Dy and Ho. Canted ferromagnetic or helical arrangements have also been found in other intermetallic systems where only the rare earth presents magnetic moment, such as Dy_6MnBi_2, Ho_6MnTe_2, Ho_6CoTe_2 [62].

In the case of pure Dy and Ho it has been also suggested that the magnetic transition might be weakly first order, as the critical exponents of the *XY*-Chiral class are very close to the Tricritical Mean

Field model ($\alpha = 0.5$, $\beta = 0.25$, $\gamma = 1$, $\delta = 5$) [56,63]. In the study presented in this paper, the experimental values of the critical exponents for Ho_3CoNi, are indeed very close to this class, save for α. Nevertheless, we discard this option since in the thermal measurements (which have been done at a very low pace, 20 mK/min) there is no hysteresis at all in heating or cooling runs and the shape of the transition is exactly the same one.

3.2. Magnetocaloric properties

In order to study the magnetocaloric properties of the five magnetic compounds of the series, magnetization isotherms have been measured from 2 K to temperatures well above T_C, as described in Section 2. The Maxwell relation has been used to calculate the magnetic entropy change as a function of temperature and magnetic field:

$$\Delta S_M(T, \Delta H) = \mu_0 \int_{H_i}^{H_f} \left(\frac{\partial M}{\partial T}\right)_H dH \quad (12')$$

The results are shown in Fig. 10 where it is seen that there is an important direct magnetocaloric effect for all of them. Table 4 presents the maximum values of the curves $|\Delta S_M^{pk}|$ for $\mu_0\Delta H = 2$, 5 and 6.9 T, together with the refrigerant capacities, calculated using the two standard definitions

$$RC_{FWHM} = |\Delta S_M^{pk}| \delta T_{FWHM}, \quad (13')$$

where $\delta T_{FWHM}$is the temperature width of the magnetic entropy change at half maximum (FWHM) and

$$RC_{Area} = \int_{T_{cold}}^{T_{hot}} \Delta S_M(T, \Delta H) dT \quad (14)$$

which is the area enclosed by the magnetic entropy change vs. temperature curve in the range enclosed by the full width at half maximum. The results at $\mu_0\Delta H = 5$ T are the ones which are more comparable with literature. We can see in Table 4 that the maximum entropy changes are 12.8, 13.6, 18.5, 15.8 and 17.1 J/Kg.K for Tb_3CoNi, Dy_3CoNi Ho_3CoNi, Er_3CoNi and Tm_3CoNi, respectively, while their RC_{FWHM} are 699, 597, 582, 449, and 412 J/Kg. If these values are compared with results shown in literature for other rare-earth based materials in their respective temperature ranges [2,5–7], they are among the highest ones, making this intermetallic family specially promising for future applications and showing that the working temperature range can be efficiently tuned by exchanging the rare earth, while maintaining good magnetocaloric properties. It would become very interesting now to investigate the possibility of mixing the rare earths to see if this working range can be efficiently displaced or extended while maintaining a high value of the maximum of the magnetic entropy change and of the refrigerant capacity, as it happens with other rare-earth intermetallic families [5,64,65].

It is worth mentioning that there is a small inverse magnetocaloric effect at very low temperature, very clear for Tb_3CoNi, small for Dy_3CoNi and Er_3CoNi and nearly negligible for Ho_3CoNi. This is related, in all cases, to a certain antiferromagnetic behavior at those temperatures. In the magnetization isotherms at low temperature it is seen that the magnetization increases (for a given field) with temperature, typical of an antiferromagnetic state (see Fig. S4 in the supplementary material). This is specially marked in the case of Tb_3CoNi, where the presence of metamagnetic transitions was already confirmed in Fig. 4. Nevertheless, the magnitude of the magnetic entropy change as well as the temperature span of these phenomena rules out any practical application.

The assignation of a particular universality class to the PM-FM can be further checked by means of the magnetocaloric variables, as there are several scaling equations that they also fulfill. In particular, the maximum of the magnetic entropy change scales with a critical exponent n which is a combination of β and δ [18,20]:

$$\Delta S_M^{pk} \sim H^{1+(1/\delta)(1-1/\beta)} = H^n \quad (15)$$

while the refrigerant capacity scales as [18,20]:

$$RC \sim H^{1+1/\delta} \quad (16)$$

Fig. 11 presents examples of these scalings for Tb_3CoNi, Dy_3CoNi, and Ho_3CoNi, using the values of β and δ previously obtained. The experimental points lie extremely well along straight lines in all cases, confirming the validity of the critical exponents contained in Table 2.

In the case of second order phase transitions, it has been shown that it is possible to build universal curves for the magnetic

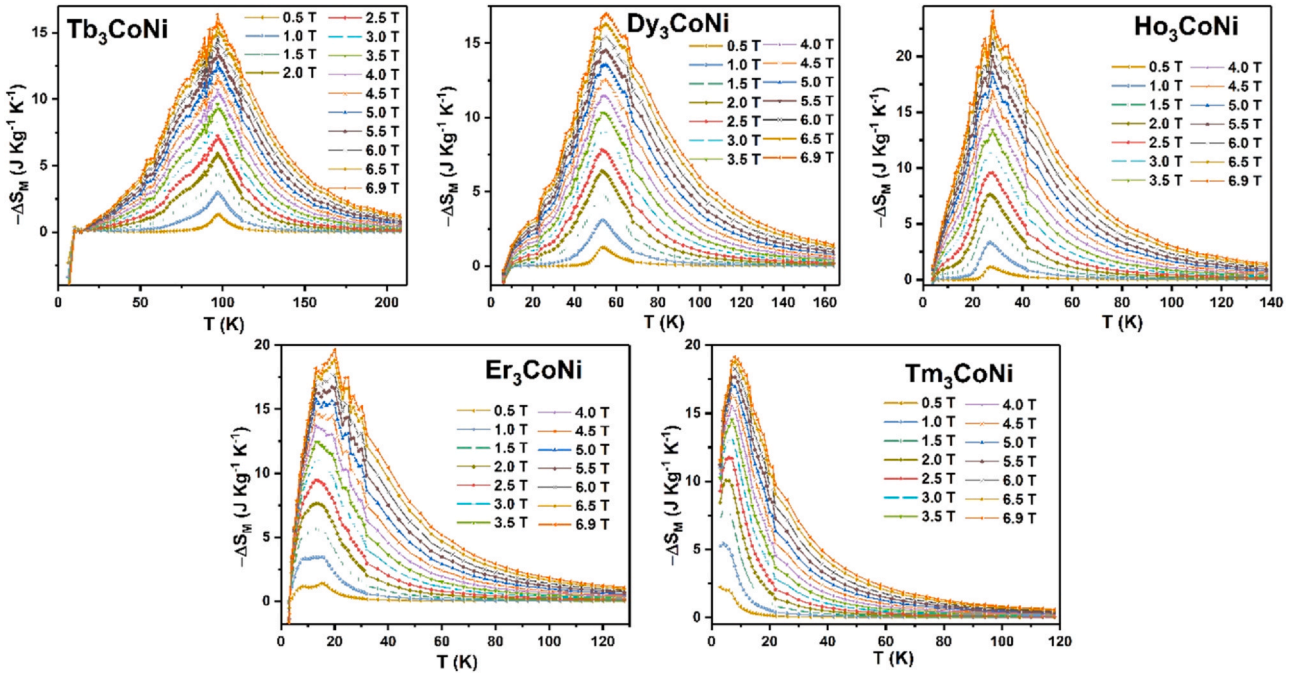

Fig. 10. Magnetic entropy change -ΔS_M for $\mu_0\Delta H$ from 0.5 T to 6.9 T for Tb_3CoNi, Dy_3CoNi, Ho_3CoNi, Er_3CoNi, and Tm_3CoNi.

Table 4
Maximum of the magnetic entropy change $|\Delta S_M^{pk}|$ and refrigerant capacities RC_{FWHM}, RC_{Area} at applied fields $\mu_0\Delta H$ (2, 5 and 6.9 T) for the five compounds. The indicated temperatures correspond to the position of the maximum of $-\Delta S_M$.

		Tb_3CoNi T_C = 97 K	Dy_3CoNi T_C = 53 K	Ho_3CoNi T_C = 27 K	Er_3CoNi T_C = 13 K	Tm_3CoNi T_C = 7 K
2 T	$\|\Delta S_M^{pk}\|$ (J kg^{-1} K^{-1}) [T_C]	5.9	6.4	7.6	7.6	10.0
	RC_{FWHM} (J kg^{-1}) [T_C]	217	166	146	152	142 [a]
	RC_{Area} (J kg^{-1}) [T_C]	152	128	113	124	-
5 T	$\|\Delta S_M^{pk}\|$ (J kg^{-1} K^{-1}) [T_C]	12.8	13.6	18.5	15.8	17.1
	RC_{FWHM} (J kg^{-1}) [T_C]	699	597	582	449	412 [a]
	RC_{Area} (J kg^{-1}) [T_C]	516	454	433	356	-
6.9 T	$\|\Delta S_M^{pk}\|$ (J kg^{-1} K^{-1}) [T_C]	16.4	17.0	24.0	19.6	19.1
	RC_{FWHM} (J kg^{-1}) [T_C]	1008	887	876	681	560 [a]
	RC_{Area} (J kg^{-1}) [T_C]	745	675	644	521	-

[a] As the magnetic entropy change peak for Tm_3CoNi is not complete on the lower temperature side, the common arrangement of considering it symmetric with respect to the maximum has been adopted to evaluate RC_{FWHM}.

entropy change in the close vicinity of the critical temperature [18]. This method implies that there is no other phase transition close enough to meddle with the first one. Therefore, this method has been applied to the case of the paramagnetic to ferromagnetic transition in Tb_3CoNi, Dy_3CoNi, and Ho_3CoNi. The magnetic entropy change is normalized with its peak value and the temperature axis is rescaled. As a first step, one reference temperature T_r is used in order to obtain a universal curve, scaling the temperature axis as follows:

$$\theta_1 = \frac{T - T_C}{T_r - T_C}. \tag{17}$$

where T_r is selected to be above T_C, corresponding to a particular fraction of $|\Delta S_M^{pk}|$, which has been chosen in these cases as 0.5. Nevertheless, it has been shown that, in many cases,
two reference temperatures T_{r1}, T_{r2} are necessary to build up the universal curves [19]. The scaling of the temperature axis in this case is as follows:

$$\theta_2 = \begin{cases} -(T - T_C)/(T_{r1} - T_C), & T \le T_C \\ (T - T_C)/(T_{r2} - T_C), & T > T_C \end{cases}. \tag{18}$$

Fig. 12 shows the result in both cases for Tb_3CoNi and Ho_3CoNi (the case of Dy_3CoNi is analogous to the last one). The overlapping must take place in the near vicinity of the second order phase transition (the critical region) [20,66], where critical theory is fulfilled, which happens both with one or two reference temperatures but better in the last case. It is generally accepted that there are two causes for the deviations when using only one reference temperature: either demagnetization effects (where the effect is that the curves below T_C move to higher values of $\frac{\Delta S_M}{\Delta S_M^{pk}}$ as the magnetic field increases [67]) or the presence of another magnetic phase with a much higher T_C than the one of the transition under study and, in this case, the curves would move to smaller values of $\frac{\Delta S_M}{\Delta S_M^{pk}}$ as the magnetic field increases [68]. In Fig. 12 it is clearly seen that the evolution of the curves at low fields is the one due to demagnetization effects, as expected, but that at fields higher than 1.6 T for Tb_3CoNi, 2 T for Dy_3CoNi and 2.8 T for Ho_3CoNi, the tendency is reversed and it is now the one described in the second case. Nevertheless, there is no trace of any other magnetic phase, neither in the X-ray nor in all the magnetic measurements performed up to room temperature. It has lately been discovered that the presence of additional magnetic phase transitions is not the only cause of the lack of universal scaling at low temperatures with that particular behavior with the field, as it has been shown that, in several single-phase Gd-alloys, the lower the critical temperature, the stronger this effect [20]. It is suggested that it might also have to do with the universality class not being a perfect Mean Field. This behavior has also been observed in other heavy rare-earths compounds such as $RTiO_3$ (R = Dy, Ho, Er, Tm, Yb) [69] or HoZn [70]. If we focus our attention on the regions far below T_C, there is a deployment of non-overlapping curves, which corresponds to temperatures well beyond the critical region, where the spin reorientation transitions have already taken place. The fact that

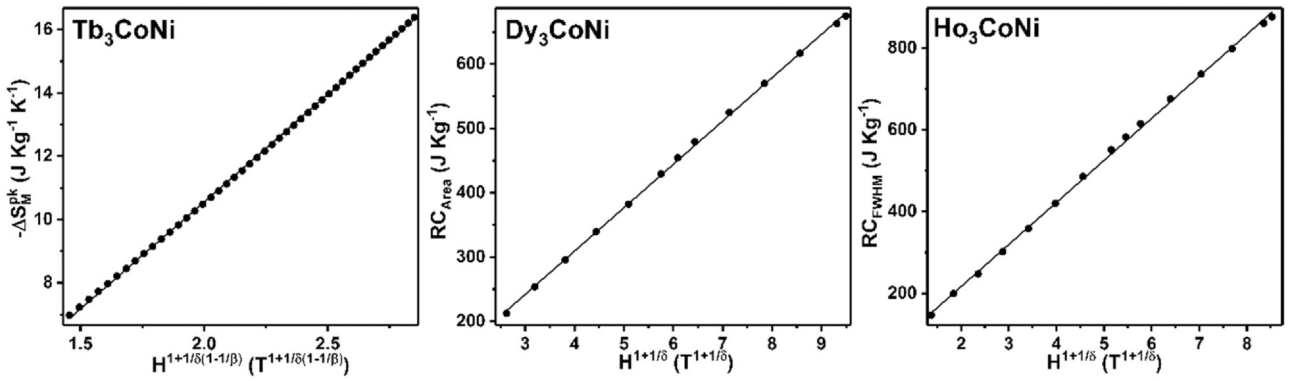

Fig. 11. Field dependence of the peak magnetic entropy change for Tb_3CoNi (left), scaling laws for the refrigerant capacity RC_{Area} for Dy_3CoNi (center) and for RC_{FWHM} for Ho_3CoNi (right) The values of β and δ used are the ones presented in Table 2.

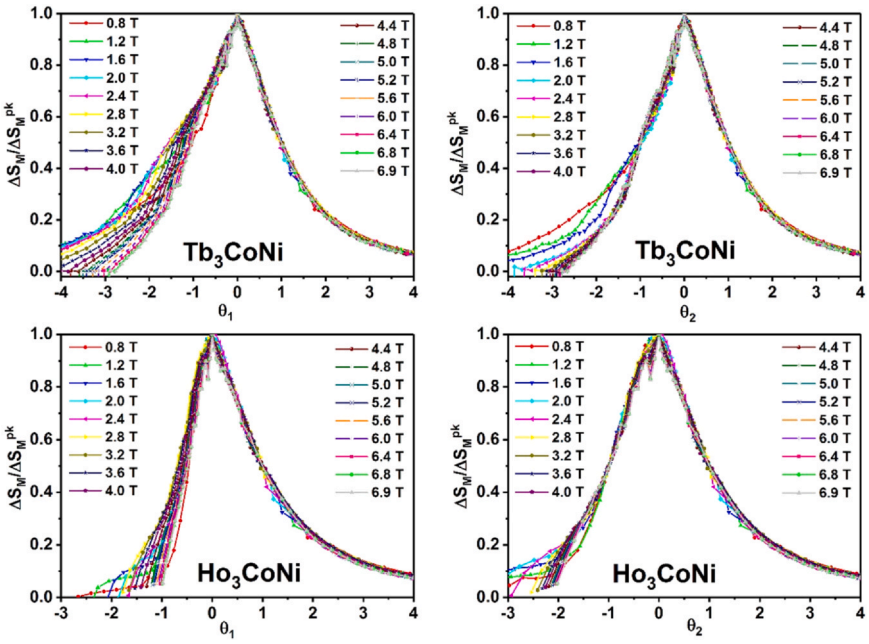

Fig. 12. Universal curve with the rescaled magnetic entropy changes using one (left) or two (right) reference temperatures, for Tb_3CoNi (above) and Ho_3CoNi (below).

these universal curves have been obtained is further proof of the second order character of the PM-FM transition in these materials.

It is worth emphasizing the usefulness of the scaling of the magnetocaloric variables, as it allows their extrapolation to different fields, which might not be experimentally accessible. Moreover, the universal curves, also called "master curves", allow the extrapolation of the whole magnetic entropy change curve to non-accessible magnetic fields [66].

4. Conclusions

The formation and crystal structure of ternary rare earth intermetallics with stoichiometry R_3CoNi have been studied. Besides the recently reported Gd_3CoNi and Tb_3CoNi, the new compounds with R = Dy, Ho, Er, Tm, and Lu have been identified; they are isomorphous, all crystallizing in the rhombohedral Er_3Ni_2-type structure. Both the lattice parameters and unit cell volume well follow the lanthanide contraction trend, with a nice linear decrease from Tb down to Lu. The magnetic and magnetocaloric properties of this novel intermetallic family R_3CoNi (R = Tb, Dy, Ho, Er, Tm) have been studied in detail showing that they all present a paramagnetic to ferromagnetic transition at temperatures in the range 96–6 K, with different reorientation transitions below the respective T_C. The decrease in T_C value from Tb to Tm compounds well follows the De Gennes scaling. The set of critical exponents (α, β, γ, δ) for this second order phase transition has been experimentally found for three cases: Tb_3CoNi, with the result that it is close to the Mean Field model, implying that long range ordering interactions rule the transition; Dy_3CoNi, between the *XY*-Chiral and Chiral Heisenberg; Ho_3CoNi, close to the *XY*-Chiral model. These two last cases suggest that they are some kind of frustrated non-collinear ferromagnets. The whole family presents very competitive magnetocaloric properties in their respective temperature ranges, with high magnetic entropy changes (from 12.8 to 18.5 J/Kg.K at $\mu_0\Delta H$ = 5 T) and refrigerant capacities (from 412 to 699 J/Kg at $\mu_0\Delta H$ = 5 T); these results indicate the possibility of tuning the application range by a proper mixing of the rare earth ions. The scaling of the magnetocaloric variables (magnetic entropy change and refrigerant capacity) for Tb_3CoNi, Dy_3CoNi, and Ho_3CoNi confirms the validity of the universality classes. Finally, universal curves for the magnetocaloric properties have also been found in these three cases.

CRediT authorship contribution statement

A. Herrero: Investigation, Software, Formal analysis, Validation, Writing - original draft. **A. Oleaga**: Supervision, Conceptualization, Methodology, Formal analysis, Validation, Writing - original draft, Writing - review & editing,. **A. Provino**: Investigation, Formal analysis**. I. R. Aseguinolaza**: Investigation, Formal analysis**. A. Salazar**: Conceptualization, Methodology, Formal analysis. **D. Peddis**: Investigation, Formal analysis. **P. Manfrinetti**: Conceptualization, Methodology, Formal analysis, Validation, Writing - original draft, Writing - review & editing.

Declaration of Competing Interest

The authors declare that they have no known competing financial interests or personal relationships that could have appeared to influence the work reported in this paper.

Acknowledgements

This work has been supported by Universidad del País Vasco UPV/EHU (project GIU19/058). A. Herrero thanks the Department of Education of the Basque Government as grantee of the programme "Programa Predoctoral de Formación de Personal Investigador No Doctor". The authors thank for technical and human support provided by SGIker of UPV/EHU.

Appendix A. Supporting information

Supplementary data associated with this article can be found in the online version at doi:10.1016/j.jallcom.2021.158948.

References

[1] A.M. Tishin, Y.I. Spichkin, The magnetocaloric effect and its applications, Series in Condensed Matter Physics, Institute of Physics Publishing, Bristol and Philadelphia, 2003.
[2] V. Franco, J.S. Blázquez, J.J. Ipus, J.Y. Law, L.M. Moreno-Ramírez, A. Conde, Magnetocaloric effect: from materials research to refrigeration devices, Prog. Mat. Sci. 93 (2018) 112–232.
[3] T. Gotschall, K.P. Skokov, M. Fries, A. Taubel, I. Radulov, F. Scheibel, D. Benke, S. Riegg, O. Gutfleisch, Making a cool choice: the materials library of magnetic refrigeration, Adv. Energy Mater. 9 (2019) 1901322.
[4] V. Franco, J.S. Blázquez, B. Ingale, A. Conde, The magnetocaloric effect and magnetic refrigeration near room temperature: materials and models, Annu. Rev. Mater. Res. 42 (2012) 305–342.
[5] Y. Zhang, Review of the structural, magnetic and magnetocaloric properties in ternary rare earth RE_2T_2X type intermetallic compounds, J. Alloy. Compd. 787 (2019) 1173–1186.
[6] H. Zhang, R. Gimaev, B. Kovalev, K. Kamilov, V. Zverev, Review on the materials and devices for magnetic refrigeration in the temperature range of nitrogen and hydrogen liquefaction, Phys. B Condens. Matter 558 (2019) 65–73.
[7] L.W. Li, Review of magnetic properties and magnetocaloric effect in the intermetallic compounds of rare earth with low boiling point, Chin. Phys. B 25 (2016) 037502.
[8] K.A. Gschneidner Jr, V.K. Pecharsky, A.O. Tsokol, Recent developments in magnetocaloric materials, Rep. Prog. Phys. 68 (2005) 1479–1539.
[9] A. Provino, V. Smetana, D. Paudyal, K.A. Gschneidner Jr, A.V. Mudring, V.K. Pecharsky, P. Manfrinetti, M. Putti, Gd_3Ni_2 and $Gd_3Co_xNi_{2-x}$: magnetism and unexpected Co/Ni crystallographic ordering, J. Mater. Chem. C 4 (2016) 6078–6089.
[10] C. Ritter, A. Provino, F. Fauth, S.K. Dhar, V.K. Pecharsky, P. Manfrinetti, From Tb_3Ni_2 to Tb_3CoNi: The interplay between chemistry, structure, and magnetism, Phys. Rev. Mater. 3 (2019) 024406.
[11] S. Gupta, K.G. Suresh, Review on magnetic and related properties of RTX compounds, J. Alloy. Compd. 618 (2015) 562–606.
[12] S.A. Nikitin, I.A. Ovtchenkova, Yu.V. Skourski, A.V. Morozkin, Magnetic properties of ternary scandium rare earth silicides and germanides, J. Alloy. Compd. 345 (2002) 50–53.
[13] A.V. Morozkin, Magnetic structures of Zr_6CoAs_2-type Ho_6FeSb_2, Ho_6CoBi_2, Ho_6FeBi_2, Ho_6MnBi_2, J. Alloy. Compd. 395 (2005) 7–16.
[14] J. Zhang, Y.M. Kang, G. Shan, S. Bobev, Structural analysis of Gd6FeBi2 from single crystal X-ray diffraction methods and electronic structure calculations, Acta Crystallogr. C75 (2019) 562–567.
[15] A.V. Morozkin, R. Nirmala, S.K. Malik, Magnetic structure of the Zr_6CoAs_2-type Er_6TX_2 compounds (T= Mn, Fe, Co and X=Sb, Bi), J. Alloy. Compd. 394 (2005) 75–79.
[16] N.V. Baranov, A.V. Proshkin, A.F. Gubkin, A. Cervellino, H. Michor, G. Hilscher, E.G. Gerasimov, G. Ehlers, M. Frontzek, A. Podlesnyak, Enhanced survival of short-range magnetic correlations and frustrated interactions in R_3T intermetallics, J. Magn. Magn. Mat. 324 (2012) 1907–1912.
[17] H.E. Stanley, Introduction to phase transitions and critical phenomena, Oxford University Press, 1971.
[18] V. Franco, A. Conde, J.M. Romero-Enrique, J.S. Blázquez, A universal curve for the magnetocaloric effect: an analysis based on scaling relations, J. Phys. Condens. Matter 20 (2008) 285207.
[19] V. Franco, J.S. Blázquez, A. Conde, Field dependence of the magnetocaloric effect in materials with a second order phase transition: A master curve for the magnetic entropy change, Appl. Phys. Lett. 89 (2006) 222512.
[20] C. Romero-Muñiz, R. Tamura, S. Tanaka, V. Franco, Applicability of scaling behavior and power laws in the analysis of the magnetocaloric effect in second-order phase transition materials, Phys. Rev. B 94 (2016) 134401.
[21] A. Herrero, A. Oleaga, A. Salazar, A.V. Garshev, V.O. Yapaskurt, A.V. Morozkin, Magnetocaloric properties, magnetic interactions and critical behavior in Ho6(Fe,Mn)Bi2 intermetallics, J. Alloy. Compd. 821 (2020) 153198.
[22] K. Yvon, W. Jeitschko, E. Parthé, LAZY PULVERIX, a computer program, for calculating X-ray and neutron diffraction powder patterns, J. Appl. Crystallogr. 10 (1977) 73–74.
[23] J. Rodriguez-Carvajal, Recent advances in magnetic structure determination by neutron powder diffraction, Phys. B 192 (1993) 55–69.
[24] H. Neves Bez, H. Yibole, A. Pathak, Y. Mudryk, V.K. Pecharsky, Best practices in evaluation of the magnetocaloric effect from bulk magnetization measurements, J. Magn. Magn. Mater. 458 (2018) 301–309.
[25] A.M. Tishin, A review and new perspectives of the magnetocaloric effect: New materials and local heating and cooling inside the human body, Int. J. Refrig. 68 (2016) 177–186.
[26] W. Jiang, X.Z. Zhou, G. Williams, Y. Mukovskii, K. Glazyrin, Critical behavior and transport properties of single crystalPr1−xCaxMnO3(x=0.27, and 0.29), Phys. Rev. B 78 (2008) 144409.
[27] W. Jiang, X.Z. Zhou, G. Williams, Y. Mukovskii, K. Glazyrin, Griffiths phase and critical behavior in single-crystalLa0.7Ba0.3MnO3: Phase diagram forLa1−xBaxMnO3(x⩽0.33), Phys. Rev. B 77 (2008) 064424.
[28] U. Zammit, S. Paoloni, F. Mercuri, M. Marinelli, F. Scudieri, Self consistently calibrated photopyroelectric calorimeter for the high resolution simultaneous absolute measurement of the specific heat and of the thermal conductivity, AIP Adv. 2 (2012) 012135.
[29] A. Oleaga, A. Salazar, D. Prabhakaran, J.G. Cheng, J.S. Zhou, Critical behavior of the paramagnetic to antiferromagnetic transition in orthorhombic and hexagonal phases of $RMnO_3$ (R = Sm, Tb, Dy, Ho, Er, Tm, Yb, Lu, Y), Phys. Rev. B 85 (2012) 184425.
[30] M. Massot, A. Oleaga, A. Salazar, D. Prabhakaran, M. Martin, P. Berthet, G. Dhalenne, Critical behavior of CoO and NiO from specific heat, thermal conductivity, and thermal diffusivity measurements, Phys. Rev. B 77 (2008) 134438.
[31] J.M. Moreau, D. Paccard, E. Parthé, The monoclinic, CrB-related, crystal structure of Tb_3Ni_2, Dy_3Ni_2 and Ho_3Ni_2, Acta Crystallogr. B 30 (1974) 2583–2586.
[32] J.M. Moreau, D. Paccard, D. Gignoux, The crystal structure of Er_3Ni_2, Acta Crystallogr. B 30 (1974) 2122–2126.
[33] P. Villars, J.L.C. Daams, Atomic-environment classification of the chemical elements, J. Alloy. Compd. 197 (1993) 177–196.
[34] F. Yuan, J. Du, B. Shen, Controllable spin-glass behavior and large magnetocaloric effect in Gd-Ni-Al bulk metallic glasses, Appl. Phys. Lett. 101 (2012) 032405.
[35] J.L. Wang, C. Marquina, M.R. Ibarra, G.H. Wu, Structure and magnetic properties of RNi2Mn compounds(R=Tb, Dy, Ho, and Er), Phys. Rev. B 73 (2006) 094436.
[36] N.K. Singh, P. Kumar, K.G. Suresh, A.K. Nigam, Investigations on magnetic and magnetocaloric properties of the intermetallic compound TbAgAl, J. Appl. Phys. 105 (2009) 023901.
[37] H. Zhang, B.G. Shen, Z.Y. Xu, J. Shen, F.X. Hu, J.R. Sun, Y. Long, Large reversible magnetocaloric effects in ErFeSi compound under low magnetic field change around liquid hydrogen temperature, Appl. Phys. Lett. 102 (2013) 092401.
[38] J.C. Debnath, J. Wang, Magnetocaloric effect in $HoMn_2Si_2$ compound with multiple magnetic phase transitions, Intermetallics 78 (2016) 50–54.
[39] A. Murtaza, W. Zuo, J. Mi, Y. Li, A. Ghani, M. Yaseen, M.T. Khan, C. Hao, K. Li, Z. Dai, S. Yang, Y. Ren, Magnetocaloric effect and critical exponent analysis around magnetic phase transition in $NdCo_2$ compound, J. Phys. D Appl. Phys. 53 (2020) 345003.
[40] A.K. Pramanik, A. Banerjee, Critical behavior at paramagnetic to ferromagnetic phase transition in $Pr_{0.5}Sr_{0.5}MnO_3$: A bulk magnetization study, Phys. Rev. B 79 (2009) 214426.
[41] A. Oleaga, A. Salazar, M. Ciomaga Hatnean, G. Balakrishnan, Three-dimensional Ising critical behavior in $R_{0.6}Sr_{0.4}MnO_3$(R=Pr,Nd) manganites, Phys. Rev. B 92 (2015) 024409.
[42] M. Campostrini, M. Hasenbusch, A. Pelissetto, P. Rossi, E. Vicari, Critical exponents and equation of state of the three-dimensional Heisenberg universality class, Phys. Rev. B 65 (2002) 144520.
[43] M. Campostrini, A. Pelisseto, P. Rossi, E. Vicari, 25-th order high-temperature expansion results for three-dimensional Ising-like systems on the simple-cubic lattice, Phys. Rev. E 65 (2002) 066127.
[44] M. Marinelli, F. Mercuri, U. Zammit, R. Pizzoferrato, F. Scudieri, D. Dadarlat, Photopyroelectric study of specific heat, thermal conductivity, and thermal diffusivity of Cr_2O_3 at the Néel transition, Phys. Rev. B 49 (1994) 9523–9532.
[45] A. Oleaga, A. Salazar, Yu.M. Bunkov, 3D-XY critical behaviour of $CsMnF_3$ from static and dynamic thermal properties, J. Phys. Condens. Matter 26 (2014) 096001.
[46] A. Oleaga, V. Liubachko, P. Manfrinetti, A. Provino, Yu Vysochanskii, A. Salazar, Critical behavior study of NdScSi, NdScGe intermetallic compounds, J. Alloy. Compd. 723 (2017) 559–566.
[47] R. Guida, J. Zinn-Justin, Critical exponents of the N-vector model, J. Phys. A Math. Gen. 31 (1998) 8103–8121.
[48] M. Campostrini, M. Hasenbusch, A. Pelisseto, P. Rossi, E. Vicari, Critical behavior of the three-dimensional XY universality class, Phys. Rev. B 63 (2001) 214503.
[49] M. Hasenbusch, Universal amplitude ratios in the three-dimensional Ising universality class, Phys. Rev. B 82 (2010) 174434.
[50] C. Bervillier, Estimate of a universal critical-amplitude ratio from itsεexpansion up toε2, Phys. Rev. B 34 (1986) 8141–8143.
[51] H. Kawamura, Universality of phase transitions of frustrated antiferromagnets, J. Phys. Condens. Matter 10 (1998) 4707.
[52] E.K. Riedel, F.J. Wegner, Tricritical exponents and scaling fields, Phys. Rev. Lett. 29 (1972) 349–352.
[53] H. Kawamura, Critical properties of helical magnets and triangular antiferromagnets, J. Appl. Phys. 63 (1988) 3086–3088.
[54] H. Kawamura, Renormalization-group analysis of chiral transitions, Phys. Rev. B 38 (1988) 4916–4928.
[55] E.H. Boubcheur, D. Loiso, H.T. Diep, Phase diagram ofXYantiferromagnetic stacked triangular lattices, Phys. Rev. B 54 (1996) 4165–4169.
[56] M.L. Plumer, A. Mailhot, Tricritical behavior of the frustrated XY antiferromagnet, Phys. Rev. B 50 (1994) 16113–16116.
[57] M.E. Fisher, S.K. Ma, B.G. Nickel, Critical exponents for long-range order interactions, Phys. Rev. Lett. 29 (1972) 917–920.
[58] Y. Ajiro, H. Kikuchi, T. Nakashima, Y. Vnno, Phase Transitions in the Frustrated ABX_3 Compounds, Jpn. J. Appl. Phys. 26 (1987) 775–776.
[59] T.E. Mason, M.F. Collins, B.D. Gaulin, Experimental confirmation of the existence of a new universality class for stacked triangular lattices, J. Phys. C Solid State Phys. 20 (1987) L945–L948.

[60] D. Gaulin, M. Hagen, H.R. Child, A critical scattering study of the helical antiferromagnets Ho and Dy, J. Phys. Colloq. 49 (1998) C8-327–328.
[61] J. Jensen, A.R. Mackintosh, Rare Earth Magnetism: Structures and Excitations, Clarendon Press, Oxford, 1991.
[62] A.V. Morozkin, R. Nirmala, S.K. Malik, Structural and magnetic properties of Fe_2P-type R_6TX_2 compounds (R=Zr, Dy, Ho, Er, T=Mn, Fe, Co, Cu, Ru, Rh, X=Sb, Bi, Te), Intermetallics 19 (2011) 1250–1264.
[63] S.W. Zachowski, D.A. Tindal, M. Kahrizi, J. Genossar, M.O. Steinitz, Critical thermal expansion of dysprosium, J. Magn. Magn. Mater. 54–57 (1986) 707–709.
[64] H. Zhang, Y.J. Sun, E. Niu, L.H. Yang, J. Shen, F.X. Hu, J.R. Sun, B.G. Shen, Large magnetocaloric effects of RFeSi (R = Tb and Dy) compounds for magnetic refrigeration in nitrogen and natural gas liquefaction, Appl. Phys. Lett. 103 (2013) 202412.
[65] A. Oleaga, A. Herrero, A. Salazar, A.V. Garshev, V.O. Yapaskurt, A.V. Morozkin, Magnetocaloric properties and unconventional critical behavior in $(Gd,Tb)_6(Fe,Mn)Bi_2$ intermetallics, J. Alloy. Compd. 843 (2020) 155937.
[66] V. Franco, A. Conde, Scaling laws for the magnetocaloric effect in second order phase transitions: from physics to applications for the characterization of materials, Int. J. Refrig. 33 (2010) 465–473.
[67] R. Caballero-Flores, V. Franco, A. Conde, L.F. Kiss, Influence of the demagnetizing field on the determination of the magnetocaloric effect from magnetization curves, J. Appl. Phys. 105 (2009) 07A919.
[68] V. Franco, R. Caballero-Flores, A. Conde, Q.Y. Dong, H.W. Zhang, The influence of a minority magnetic phase on the field dependence of the magnetocaloric effect, J. Magn. Magn. Mater. 321 (2009) 1115–1120.
[69] Y. Su, Y. Sui, J.-G. Cheng, J.-S. Zhou, X. Wang, Y. Wang, J.B. Goodenough, Critical behavior of the ferromagnetic perovskites RTiO3 (R = Dy, Ho, Er, Tm, Yb) by magnetocaloric measurements, Phys. Rev. B 87 (2013) 195102.
[70] L. Li, Y. Yuan, Y. Zhang, R. Pöttgen, S. Zhou, Magnetic phase transitions and large magnetic entropy change with a wide temperature span in HoZn, J. Alloy. Compd. 643 (2015) 147–151.